Redox Biology 69 (2024) 103013

Contents lists available at ScienceDirect

Redox Biology

journal homepage: www.elsevier.com/locate/redox

Endothelial TET2 regulates the white adipose browning and metabolism via fatty acid oxidation in obesity

Yefei Shi [a,1], Xinru Huang [b,1], Yanxi Zeng [a,1], Ming Zhai [a], Hongyun Yao [b], Chang Liu [c], Bo Li [a], Shiyu Gong [a], Qing Yu [a], Jianhui Zhuang [a], Yifan Zhao [a], Liesheng Lu [d], Bo Zhou [e], Weixia Jian [b,**], Wenhui Peng [a,*]

[a] Department of Cardiology, Shanghai Tenth People's Hospital, Tongji University School of Medicine, Shanghai, China
[b] Department of Endocrinology, Xinhua Hospital, Shanghai Jiaotong University School of Medicine, Shanghai, China
[c] Eye Institute and Department of Ophthalmology, Eye & ENT Hospital, Fudan University, Shanghai, China
[d] Department of Endocrinology and Metabolism, Shanghai Tenth People's Hospital, Tongji University School of Medicine, Shanghai, China
[e] Department of General Surgery, Shanghai Tenth People's Hospital, Tongji University School of Medicine, Shanghai, China

ARTICLE INFO

Keywords:
TET2
Obesity
Fatty acid oxidation
BMP4
NRF2

ABSTRACT

Obesity is a complex metabolic disorder, manifesting as excessive accumulation of body fat. Ten-Eleven Translocation-2 (TET2) has garnered significant attention in the context of obesity due to its crucial role in epigenetic regulation and metabolic homeostasis. In this study, we aimed to investigate the effect of endothelial TET2 on obesity and explore the potential mechanism. We generated endothelial cell-specific TET2 deficiency mice and investigated endothelial TET2 using transcriptomic and epigenomic analyses. We determined the downregulation of endothelial TET2 in white adipose tissues. Furthermore, we identified that endothelial TET2 loss aggravated high-fat diet-induced obesity by inhibiting vascularization and thus suppressing white adipose tissue browning. Mechanistically, endothelial TET2 modulates obesity by engaging in endothelial fatty acid oxidation and angiocrine-mediated secretion of bone morphogenetic protein 4 (BMP4), in which nuclear factor-erythroid 2-related factor 2 (NRF2) serves as a key mediator. Our study reveals that endothelial TET2 regulates white adipose tissue browning by interacting with NRF2 to facilitate fatty acid oxidation and lipolysis in adipocytes.

1. Introduction

Obesity, a multifaceted metabolic disorder, manifests as the excessive accumulation of body fat, precipitating a range of chronic complications, such as cardiovascular disease, type 2 diabetes mellitus, and cancer [1,2]. The global prevalence of obesity has surged dramatically as population aging, presenting a significant public health challenge [3]. Notably, obesity is characterized by the substantial expansion of adipocytes, disrupting the equilibrium of adipokine secretion, provoking chronic inflammation, and fostering tissue fibrosis. Within the context of obesity, adipose tissue remodeling commonly entails a reduction in capillary density, which impairs oxygen delivery, nutrient absorption, and signaling molecular production [4,5]. Consequently, this compromised microenvironment triggers adipocyte dysfunction and instigates insulin resistance.

Endothelial cells (ECs) are extensively distributed throughout the body, forming a pivotal interface between the bloodstream and tissues. This interface enables the precise detection of environmental cues, efficient nutrient transport, and the integration of signaling from neighboring tissues [6]. Given the powerful function of ECs in blood vessels, vascular therapy targeting ECs is a potential treatment for obesity [7]. Accordingly, Kai Sun et al. demonstrated that the local up-regulation of vascular endothelial growth factor (VEGF) in adipose tissue could improve high-fat diet (HFD)-induced weight gain via

* Corresponding author. Department of Cardiology, Shanghai Tenth People's Hospital, Tongji University School of Medicine, 301 Middle Yanchang Road, Shanghai, 200072, China.
** Corresponding author. Department of Endocrinology, Xinhua Hospital, Shanghai Jiaotong University School of Medicine, 1665 Kongjiang Road, Shanghai, 200092, China.
E-mail addresses: jianweixia@xinhuamed.com.cn (W. Jian), pwenhui@tongji.edu.cn (W. Peng).
[1] Co-first author.

https://doi.org/10.1016/j.redox.2023.103013
Received 14 November 2023; Received in revised form 19 December 2023; Accepted 23 December 2023
Available online 28 December 2023

angiogenesis [8]. Grunewald et al. also revealed that age-associated adverse alterations in adipose tissue were ameliorated by VEGF treatment, where VEGF functioned as an angiogenic stimulator [9]. Despite their indispensable role, ECs remain unknown as to their specific contributions in regulating systemic metabolism and their possible involvement in metabolic disorders.

Ten-Eleven Translocation 2 (TET2), an epigenetic regulator, facilitates DNA demethylation by converting 5-methylcytosine to 5-hydroxymethylcytosine [10,11]. Mutations in the TET2 gene are frequently found in clonal hematopoiesis of indeterminate potential [12,13], and dysfunction of myeloid TET2 exacerbates insulin resistance in aging and obesity [14]. Our previous study showed that endothelial TET2 could regulate angiogenesis and improve the prognosis of ischemic diseases. However, it remains unclear whether the functional deficiency of endothelial TET2 can also influence obesity and insulin resistance.

In this study, we performed a comprehensive experiment on the involvement of endothelial TET2 in obesity. Our findings elucidated that the deficiency of TET2 in ECs led to a decline in the proliferation of the vascular compartment within the white fat tissue (WAT), consequently exacerbating adiposity. Through endothelial fatty acid oxidation (FAO), endothelial function is intertwined with adipocyte biology. We present compelling evidence that highlights the significance of TET2/FAO metabolic axis in obesity.

2. Material and methods

2.1. Animals

Mice were maintained under controlled conditions of temperature (25 ± 1 °C) and humidity-controlled facility under a reversed 12 h dark/light cycle. C57BL/6J mice were purchased from Vital River Laboratory. CDH5Cre mice (B6-Cdh5$^{tm1(iCre/ERT2)}$/Bcgen) were purchased from Biocytogen Co., Ltd. TET2-floxed mice (B6; 129S-Tet2$^{tm1.1Iaai}$/J) were purchased from the Jackson Laboratory. CDH5Cre (+) mice and TET2-$^{flox/flox}$ mice continuously bred to obtain CDH5Cre (+)-TET2$^{flox/flox}$ mice, and tamoxifen (75 mg/kg body weight, Cat#T5648, Sigma-Aldrich) was injected for 5 consecutive days to acquire endothelial cell-specific TET2 knockout (TET2^{EC-KO}) mice. 8-week-old TET2$^{flox/flox}$ (referred to as wild type, WT) and TET2^{EC-KO} male mice were fed with either a standard chow diet or HFD, containing 60 kcal% fat (D12492, Research Diets) for 16 weeks. Subcutaneous adipose tissue (SAT) from the inguinal region and visceral adipose tissue (VAT) adjacent to the epididymis of mice were taken for study. Mice were anaesthetized with isoflurane (2 %) through nose inhalation for the duration of the surgeries and with CO_2 for euthanasia. All the animal experiments were conducted in accordance with the National Research Council's Guide for the Care and Use of Laboratory Animals, and were approved by the Animal Care and Use Committee of Shanghai Tenth People's Hospital (Approval NO. SHDSYY-2020-2149).

2.2. Human samples

All participants were given informed consent prior to the inclusion and this study was conformed to the principles outlined in the Declaration of Helsinki. The Ethics Committee of the Tenth People's Hospital in Shanghai approved this study (Approval NO. SHSY-IEC-5.0/23KY13/P01). We recruited 7 young individuals with a normal BMI (Age, 34.7 ± 2.3 years; BMI, 22.9 ± 1.1 kg/m^2, mean ± SEM), 10 young individuals with obesity (Age, 28.1 ± 1.6 years; BMI, 43.0 ± 2.9 kg/m^2, mean ± SEM) and 9 old individuals with a normal BMI (Age, 72.2 ± 5.5 years; BMI, 22.3 ± 2.5 kg/m^2, mean ± SEM). The characteristics of patients were listed in Supplementary Table 1. Adipose tissues of the obese group were taken from patients who underwent fat reduction surgery at the Weight Loss Center of the Shanghai Tenth People's Hospital, while the elderly and non-obese groups were taken from patients who underwent cholecystectomy for gallstones in the Hepatobiliary Department of the Shanghai Tenth People's Hospital. Human SAT was taken from the patient's abdominal subcutaneous tissue, while VAT was taken from the patient's omental adipose tissue. Exclusion criteria were previous bariatric surgery, tumor cachexia, severe liver and kidney dysfunction, and severe inflammation.

2.3. Body composition and energy balance measurement

A magnetic resonance imaging technique (EchoMRI Body Composition Analyzer E26-245-M) was used to determine murine body composition. Each mouse was scanned for 1–2 min without anesthesia. Total fat mass and total lean mass were further calculated to compare the differences between different genotypes. To conduct the energy balance measurement, we allocated three days to house the mice in metabolic cages under controlled lighting and temperature conditions. Food and water were freely available. Using metabolic cages, food intake, physical activity, respiratory exchange ratio, and energy expenditure were measured.

2.4. Glucose tolerance test and insulin tolerance test

A glucose tolerance test was performed on mice following a 12-h fast and intraperitoneal administration of glucose (2 g/kg body weight) intraperitoneally. Glucose levels were measured at 0, 15, 30, 60, 90 and 120 min by sampling from the tail vein. An insulin tolerance test was conducted on mice after fasting for 6 h. Intraperitoneal insulin (0.75 U/kg body weight) was administered and blood glucose levels were monitored at 0, 15, 30, 60, 90, and 120 min in the experiment.

2.5. RNA isolation and RT-qPCR

Total RNAs were extracted from cells and tissues using TRIzol Reagent (Cat#15596026, Invitrogen). 1 μg total RNA was reversely transcribed using HiScript III RT SuperMix (Cat#R323, Vazyme), and cDNAs were used for qPCR analyses (Roche LightCycler96) using the primers listed in Supplementary Table 2.

2.6. DNA isolation and methylation-specific PCR (MSP)

Genomic DNA was isolated using TIANamp Genomic DNA Kit (Cat#DP304, TianGen). The isolated DNA was treated with sodium bisulfite and MSP reactions were carried out using TaKaRa Ex Taq® Hot Start Version (Cat#RR006, Takara). The primers used for MSP were listed in Supplementary Table 2.

2.7. Histology, immunofluorescence and immunohistochemical analysis

Tissues from mice were embedded in paraffin wax, cut into sections, and then deparaffinized. Then specimens were stained with hematoxylin and eosin (H&E). Tissue sections were incubated in 10 % goat serum and 0.5 % Triton-X 100, and stained by primary antibodies (listed in Supplementary Table 3). DAPI (1:5000, Vector Laboratories) was used to stain the cell nuclei. Adipose cells and frozen liver sections were stained with Oil Red O for hydrophobic and neutral lipids, and the nuclei were then stained with hematoxylin. Images were obtained using the Olympus IX83 fluorescence microscope (Olympus Corporation, Japan). The positive area values of sections were quantified by ImageJ software (v1.52a, National Institutes of Health).

2.8. Western blot analysis

Cell and adipose samples were lysed in Cell Lysis Buffer (Cat#9803s, Cell Signaling Technologies) and quantified using the BCA Protein Quantification Kit (Cat#20201ES76, Yeasen). A total of 30 μg protein was separated by SDS-PAGE and then transferred onto PVDF membranes. The membranes were blocked at room temperature for 1 h, then

incubated with primary antibodies at 4 °C overnight. On the second day, the membranes were incubated with HRP-conjugated secondary antibodies at room temperature for 1 h and exposed to ECL exposure solution (Cat#180–5001, Tanon). Then, using the Amersham Imager 600 system (GE Healthcare, USA) to develop the membrane. The primary and secondary antibodies used were listed in Supplementary Table 3.

2.9. CL316243, BMP4 recombinant protein, acetate and adenovirus injection

To administer β (3)-adrenaline receptor agonist treatment, CL316243 (1 mg/kg, HY-116771A, MedChemExpress) was injected intraperitoneally into 8-week C57BL6/J mice for 7 consecutive days. For gain of function, BMP4 recombinant protein (50 μg/ml, HZ-1045, Proteintech) was injected point-to-point into 3 sites of SAT with a micro syringe, sham operation was performed in the control group. Acetate (20 mM, Cat#S2889, Sigma-Aldrich) was injected point-to-point into 3 sites of SAT with a micro syringe, sham operation was performed in the control group. For adenovirus (Ad) injection, AdNC or Ad-TET2 (10^{11} PFU/ml) was injected into the SAT of mice. Each SAT was injected with 3 spots.

2.10. Cell culture and stimulation

Human umbilical vein endothelial cells (HUVECs), purchased from Sciencell Research Laboratories (Cat#8000, ScienCell), were cultured in ECM (Cat#1001, ScienCell) supplemented with 5 % FBS (Cat#0025, ScienCell), 1 % ECGS (Cat#1052, ScienCell) and 1 % P/S (Cat#0503, ScienCell) at 37 °C in 5 % CO_2. HUVECs were stimulated with D-glucose (33.3 mM, Cat#G8644, Sigma-Aldrich), tumor necrosis factor (TNF-α, 10 ng/ml), lipopolysaccharide (LPS, 100 ng/ml, Cat#L3024, Sigma-Aldrich), phorbol myristate acetate (PMA, 100 nM, Cat# S1819, Beyotime Biotechnology), and palmitic acid (PA, 100 μM, Cat#P5585, Sigma-Aldrich) for 48 h. Human embryonic kidney 293 T (HEK293T, Shanghai Zhongqiaoxinzhou Biotechnology) cells were cultured in DMEM with 10 % FBS and 1 % P/S.

2.11. siRNA knockdown and plasmid transfection

Small interfering RNAs (siRNAs, 50 nM) were transfected into HUVECs using jetPRIME (Cat#114, Polyplus-transfection) according to the introduction. The sequences of siRNAs were listed in Supplementary Table 2. The plasmids of TET2 and NRF2 were constructed by Shanghai Genomeditech Co., Ltd. and transfected into HEK293T using Lipofectamine 2000 (Cat# 11668027, Invitrogen).

2.12. Induction of adipocytes and indirect contact co-culture with ECs

3T3-L1 cells (Shanghai Zhongqiaoxinzhou Biotechnology) were cultured in DMEM with 10 % FBS and 1 % P/S. After post-confluence, cells were incubated with medium (DMEM with 10 % FBS and 1 % P/S) containing inductive agents (10 μg/ml insulin, 1 μM dexamethasone, 0.5 mM 3-isobutyl-1-methylxanthine and 1 μM rosiglitazone) for 2 days. Then mature adipocytes were cultured in DMEM medium with 10 μg/ml insulin for the following 7 days. For cell co-culture, bEnd.3 cells were seeded in the upper chambers (Cat#3412, Corning) and transfected with adenoviruses for 2 days. Then bEnd.3 cells were transferred to a culture plate containing mature adipocytes and co-cultured for 48 h.

2.13. In vivo WAT explants and free fatty acid (FFA) assay

Fresh white adipose tissues from mice were collected in precooled DMEM (containing 1 g/L glucose and 0.5 % FFA-free BSA) and cut into small pieces. 25 mg of samples were placed in 24-well plates with 500 μl of DMEM (containing 1 g/L glucose and 0.5 % FFA-free BSA) and incubated at 37 °C. For FFA determination, aliquots of media were taken at 0 and 120 min. FFA concentration was qualified using Free Fatty Acid Test Kit (Cat#ml092765, Enzyme-linked Biotechnology) following the manufacturer's instruction.

2.14. Human adipokine assay

The Human Adipokine Array Kit (Cat#ARY024, R&D Systems) was used to measure the levels of adipokines in supernatants in accordance with the manufacturer's instructions. Nitrocellulose membranes, spotted with capture and control antibodies, were incubated in array block buffer at room temperature for 1 h. Samples were mixed with reconstituted human adipokine detection antibody cocktail and incubated at room temperature for 1 h. Next, the mixtures were incubated with the membrane overnight at 4 °C. After washing 3 times, the membrane was incubated in 2 ml diluted streptavidin-HRP for 30 min at room temperature. At last, the membrane was exposed by the Amersham Imager 600 system (GE Healthcare, USA).

2.15. ELISA assay

Insulin, BMP4 and global DNA methylation levels were measured by murine INS ELISA kits (Cat#YCQZ-10385, YC Bio), murine BMP4 ELISA kits (Cat#EK0316, Boster), and Global DNA Methylation–LINE-1 Kit (Cat#55017, Active Motif) respectively. Firstly, the standard product, samples and HRP-conjugated streptavidin were added into designated wells and incubated at 37 °C for 1 h. After washing, the substrate solution was added to the wells and incubated at 37 °C for 15 min. Finally, absorbance optical density was read at 450 nm using a microtiter plate reader (SpectraMax i3, Molecular Devices).

2.16. GSEA

Gene set enrichment analysis (GSEA, version 4.1.0) was used to determine whether the gene-defined genomes between HUVECs transfected with control siRNA and TET2 siRNA under hypoxia for 48 h were statistically significant. RNK file based on genes' log2Fold-Change and -log10P.value was constructed. GSEA was performed using a default algorithm of 1000 permutations, with a minimum term size of 15 and a maximum term size of 500. HALLMARK was collected from the Molecular Signature Database 3.0. and used as our annotated gene set. Enriched gene sets were assigned according to normalized p value < 0.05 and FDR q value < 0.25 (Accession Number: GSE200080).

2.17. Co-immunoprecipitation

HUVECs or HEK293T were lysed with cell lysis buffer (Cat#9803, Cell Signaling Technologies) with protease inhibitors (Cat#04693159001, Roche) and quantified using the BCA Protein Quantification Kit (Cat#20201ES76, Yeasen). 500 μg protein was incubated with the primary antibodies at 4 °C overnight. Subsequently, the cell lysate was purified with 20 μl protein A/G agarose (Cat#sc-2003, Santa Cruz) at 4 °C for 4 h. The resulting protein was used for western blotting. The antibodies were listed in Supplementary Table 3.

2.18. CUT & tag assay

CUT & Tag of HUVECs was operated by Hyperactive Universal CUT & Tag Assay Kit for Illumina (Cat#TD903, Vazyme) as described previously with minor modifications [15]. A total of 1×10^5 cells were washed twice gently with wash buffer, then 10 μl concanavalin A-coated magnetic beads were added to each sample and incubated at room temperature for 10 min. After discarding the unbound cells, the bound cells were mixed with an anti-TET2 antibody (1:100, ab230358, Abcam) or rabbit normal IgG antibody (1:200, Cat#2729, CST) and incubated at 4 °C overnight with rotation. Next, cells were incubated in a secondary antibody, which was diluted in DIG wash buffer at room temperature for

1 h, and washed 3 times in DIG wash buffer. The beads were incubated with a pA/G-Tnp adapter complex (0.04 μM) at room temperature for 1h with rotation and washed 3 times in DIG-300 buffer. DNA was purified using phenol-chloroform isoamyl alcohol extraction and ethanol precipitation. To amplify the library, 15 μl purified DNA was mixed with 5 μl of a universal i5 and a uniquely barcoded i7 primer. A volume of 25 μl 2 × CUT & Tag amplification mix was added and mixed. The sample was placed in a PCR thermal cycler with a heated lid using the following program: 72 °C for 3 min; 95 °C for 3 min; 18 cycles of 98 °C for 10 s and 60 °C for 5 s; final extension at 72 °C for 1 min and hold at 4 °C.

2.19. Statistical analysis

Data in this study were shown as the mean ± SEM (Standard Error). Unpaired Student's two-tailed *t*-test was used to compare the two groups of samples if data had equal variance and Mann–Whitney test was used to analyze if data had unequal variance. One-way or two-way ANOVA was used to determine statistical significance for more than two groups of samples. $P < 0.05$ was considered statistically significant. All statistical analysis was performed using GraphPad Prism (v6.01, GraphPad Software).

3. Results

3.1. TET2 expression in adipose ECs is reduced by obesity

To determine in which organ ECs may play an important role, we first analyzed the single-cell profiling of Olga Bondareva et al. [16], which contained ECs of multiple organs in HFD-induced obesity model, including brain, heart, lung, kidney, liver, SAT and VAT (Fig. 1A). The analyzed results indicated that the number of ECs in SAT and VAT increased significantly with the development of obesity (Fig. 1B). Meanwhile, ECs in adipose tissue, including SAT and VAT showed the most different expression genes (Fig. 1C), which suggested that an epigenetic regulator may play a crucial role in this progress. As our previous study, TET2 could play the role of DNA demethylase in regulating gene expression in ECs [17]. To investigate the presence of aberrant endothelial TET2 expression in adipose tissue, we conducted TET2 staining on adipose tissue from mice with HFD-induced obesity. As expected, the expression of TET2 was decreased in SAT (Fig. 1D and E) and VAT (Fig. 1F and G) from HFD-induced obese mice, and TET2 was significantly colocalized with the EC marker (IB4). We further observed the downregulation of TET2 in SAT (Fig. 1H and I) and VAT (Fig. 1J and K) from obese patients. Similarly, comparable reduction of TET2 was found in aging mice (Supplementary Figs. S1A–D) and people (Supplementary Figs. S1E–H). Consistent with the in-vivo experiments, TET2 expression was reduced in HUVECs after stimulation with glucose, TNF-α, LPS, PMA or PA (Fig. 1L and M). Because Akt and eNOS phosphorylation were the pivotal pathways of insulin sensitivity, the phosphorylated levels of AKT and eNOS were examined in HUVECs transfected with or without TET2 siRNA. TET2 knockdown inhibited the phosphorylation of AKT and eNOS (Fig. 1N and O). These data suggested that endothelial TET2 was reduced in obesity.

3.2. Loss of endothelial TET2 aggravates HFD-induced obesity

To examine the effect of endothelial TET2 on metabolism, we generated endothelial-specific TET2 deficiency mice ($TET2^{EC-KO}$) (Fig. 2A) and identified the genotypes by PCR (Fig. 2B). ECs ($CD31^{+}CD45^{-}$), non-ECs of stromal vascular fraction (SVF) and mature adipocyte fraction (MAF) were sorted from SAT (Supplementary Fig. S2A) and we confirmed that TET2 expression was successfully reduced by tamoxifen (Fig. 2C) without influence on TET1 or 3 (Supplementary Fig. S2B) in ECs, as well as no influence on TET2 in MAF (Supplementary Fig. S2C) and non-ECs of SVF (Supplementary Fig. S2D). It was further confirmed by immunofluorescence that TET2 was significantly decreased in ECs in SAT and VAT (Supplementary Figs. S2E–H). Then, HFD was used to mimic a fast-food diet and insulin resistance in humans. Consistent with previous study [18], wild-type (WT) mice fed with HFD gained more weight than mice with a chow diet over time. In chow diet group, no noticeable distinctions were observed in terms of body weight, organ weight, food intake, fasting glucose levels or triglycerides between WT mice and $TET2^{EC-KO}$ mice (Supplementary Figs. S3A–E). Following 16 weeks of HFD, $TET2^{EC-KO}$ mice exhibited a significant weight gain, compared with WT mice (Fig. 2D and E). Interestingly, $TET2^{EC-KO}$ mice had a remarkable difference in body weight accompanied by an increase in body fat mass and a decrease in lean mass (Fig. 2F). In addition to being highly sensitive to HFD-induced obesity, $TET2^{EC-KO}$ mice showed more severe glucose intolerance and insulin resistance (Fig. 2G and H). We further assessed the weights of the major metabolic organs and revealed that the increased weights of SAT and VAT exhibited the most noticeable changes (Fig. 2I and J). Surprisingly, we found that endothelial TET2 deficiency exacerbated obesity induced by HFD.

3.3. Endothelial TET2 deficiency disrupts metabolism and WAT browning in HFD-induced obesity

To determine how the deficiency of endothelial TET2 aggravates obesity, we monitored the factors involved in obesity, including nutritional uptake, energy consumption and metabolic rate in the mouse model. Of note, there were no differences in food or water intake and locomotor activity (Supplementary Figs. S4A–F). Although plasma insulin level was also an important factor in obesity [19], the insulin levels of WT and $TET2^{EC-KO}$ mice were similar (Supplementary Fig. S4G). Furthermore, the metabolic levels of mice were investigated to explain the deteriorated metabolic phenotype. Interestingly, there were lower rates of oxygen consumption (VO_2), carbon dioxide production (VCO_2), and energy expenditure in the $TET2^{EC-KO}$ mice in both light and dark cycles (Fig. 3A–C). It was determined that the deficiency of endothelial TET2 disrupts the metabolism.

Considering that SAT and VAT had the most significant variation in weight, we hypothesized that white adipose tissue played a major role in this metabolic phenotype. We further found that the sensitivity of SAT and VAT to insulin was worsened in the $TET2^{EC-KO}$ mice (Fig. 3D and E). Previous studies demonstrated that TET2 could regulate inflammation in some diseases, such as atherosclerosis [20], heart failure [21] and gout [22]. Therefore, the effect of endothelial TET2 deletion on adipose inflammation in obese mice was examined. First, macrophage content indicated by Mac2 staining in SAT and VAT was not significantly changed in $TET2^{EC-KO}$ mice under HFD (Supplementary Figs. S5A and B). Second, the M1 and M2 markers of macrophage were examined using qPCR. The deficiency of TET2 in ECs did not significantly change the expression of the macrophage M1 or M2 markers in SAT and VAT (Supplementary Figs. S5C and D). To determine the effect of endothelial TET2 deficiency on WAT, the browning phenotypes of SAT and VAT were assessed. We found an increase in the adipocyte area of SAT and VAT, as well as a decrease in the density of blood vessels and the expression level of UCP1 in $TET2^{EC-KO}$ mice fed with HFD (Fig. 3F–I). In addition, several hallmark genes governing browning and thermogenesis were also decreased, including UCP1, Cox8b and Ppargc1a (Fig. 3J and K). The β-adrenergic activator CL316243 is an activator of adipose browning, which could induce adipose angiogenesis in SAT and VAT [23,24]. It was also observed lower levels of browning in SAT and VAT of $TET2^{EC-KO}$ mice after treatment with CL316243 (Supplementary Figs. S6A and B). The results suggested that the deficiency of TET2 in ECs suppressed the metabolism and WAT browning.

3.4. Endothelial TET2 modulates lipolysis through secretion of BMP4

As the forefront of distribution and nutrient sensing, ECs could influence adipose browning through cytokines [25]. We hypothesized that

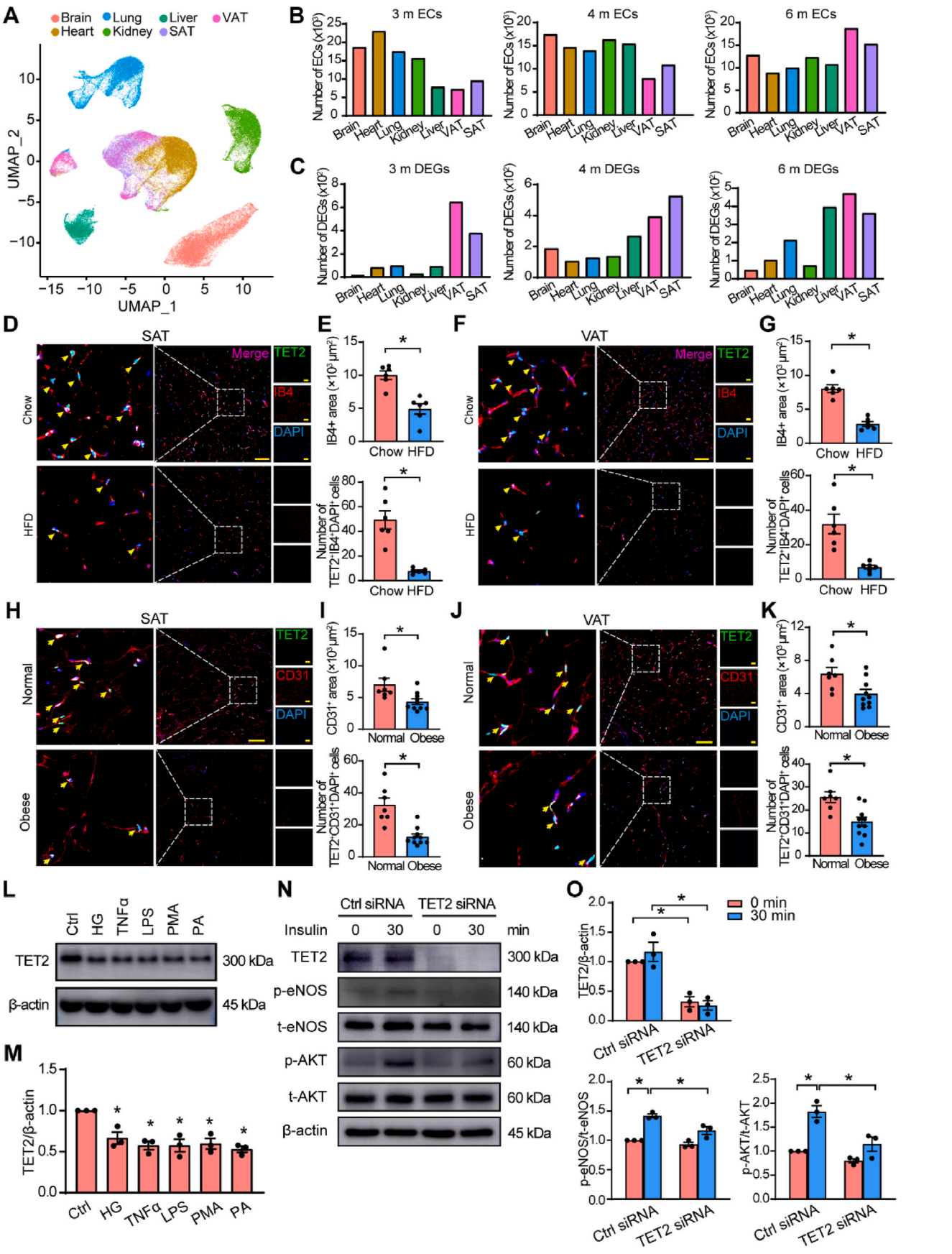

(caption on next page)

Fig. 1. TET2 expression in adipose ECs is reduced by obesity. A, UMAP of single cell profile with each cell color-coded for ECs of each sample type. **B**, Numbers of ECs in different organs with different times of HFD. **C**, Number of different expression genes in ECs from different organs with different times of HFD. **D** and **F**, Representative images of SAT (D) and VAT (F) for staining with TET2 (green), IB4 (red) and DAPI (blue) from mice fed with chow diet or HFD for 16 weeks. Scale bar = 50 μm. **E** and **G**, Quantification of IB4-positive area and number of cells (TET2, CD31 and DAPI triple-positive) in SAT (D) and VAT (F). n = 6 mice/group. **H** and **J**, Representative images of SAT (H) and VAT (J) for staining with TET2 (green), CD31 (red) and DAPI (blue) from normal and obese people. Scale bar = 50 μm. **I** and **K**, Quantification of CD31-positive area and number of cells (TET2, CD31 and DAPI triple-positive) in SAT (H) and VAT (J). n of normal group = 7 people, n of obese group = 10 people. **L**, Western blot analysis of HUVECs treated with multiple stimulations. n = 3/group. **M**, Quantification of L. **N**, Western blot analysis of Akt and eNOS phosphorylation in HUVECs transfected with Ctrl siRNA or TET2 siRNA. n = 3/group. **O**, Quantification of M. All data are mean ± SEM. E, G, I, K, unpaired Student's *t*-test; M, one-way ANOVA with Bonferroni post hoc test; O, two-way ANOVA with Bonferroni post hoc test. $^{*}P < 0.05$. (For interpretation of the references to color in this figure legend, the reader is referred to the Web version of this article.)

the changed secretion of cytokines led to reduced lipolysis of adipocytes in $TET2^{EC-KO}$ mice. To investigate this, we quantified the basal and stimulated fatty acid secretion into the media of both WT and $TET2^{EC-KO}$ mice (Fig. 4A). Explants from the SAT and VAT of $TET2^{EC-KO}$ mice exhibited a lower release of FFAs than WT mice (Fig. 4B and C). Furthermore, the role of endothelial TET2 in adipocytes was verified in vitro (Fig. 4D). After successful overexpression of TET2 in ECs (Fig. 4E) and induction of adipocytes differentiation (Supplementary Figs. S7A and B), we performed ECs co-culture experiments with 3T3-L1-induced adipocytes. Adipocytes co-cultured with TET2 overexpressed ECs exhibited reduced lipid droplets, as revealed by Oil Red O staining, along with increased expression of lipolysis genes in adipocytes (Fig. 4F and G). To find out which cytokine was regulated by TET2, a proteome profiler adipokine array was conducted. The adipokine array assay showed that BMP4 was the most significantly decreased cytokine in TET2-silenced ECs (Fig. 4H and I). Meanwhile, the mRNA level of BMP4 was also decreased in ECs, accompanied by the knockdown of TET2 (Fig. 4J). In addition, we observed a decrease in the serum expression level of BMP4 in $TET2^{EC-KO}$ mice compared to WT mice (Fig. 4K). BMP4 is associated with numerous pathologies, including obesity, diabetes, and related complications [26]. To determine whether BMP4 could explain the metabolic effect of endothelial TET2 deficiency, we conducted cell co-cultures of ECs and adipocytes, with or without recombinant BMP4 protein. The results showed that recombinant BMP4 protein slightly upregulated the expression level of lipolysis genes in adipocytes, such as Lipe and Pnpla2 (Supplementary Fig. S7C). We further orthotopically expressed BMP4 using recombinant protein in the SAT of $TET2^{EC-KO}$ mice subject to the CL316243 treated mice. The successful overexpression of BM4 was first confirmed in WT mice (Supplementary Fig. S8). To further prove that the loss of TET2 in ECs leaded to reduced browning by inhibiting the secretion of endothelial BMP4, recombinant BMP4 proteins were injected into the local adipose tissue of $TET2^{EC-KO}$ mice treated with CL316243. Interestingly, the recovery of the browning phenotype was not observed (Fig. 4L and M).

3.5. TET2 regulates WAT browning via FAO in ECs

Although BMP4 was supplied in $TET2^{EC-KO}$ mice, the browning of WAT did not recover, especially the density of blood vessels. After analyzing our previous RNA sequencing datasets (GSE200080), fatty acid metabolism was found to be reduced in TET2 knockdown ECs (Fig. 5A and B). We evaluated the expression of lipid catabolism-related genes in adipose tissue with the deficiency of endothelial TET2. The deficiency of endothelial TET2 resulted in the down-regulation of genes associated with fatty acid transporters, which played a crucial role in FAO and served as central regulators of cellular energy metabolic pathways (Fig. 5C). As FAO was essential for EC proliferation [26,27], the effect of TET2 on FAO in ECs was detected. With the silence of TET2, the ability of ECs to use exogenous fatty acids for FAO was decreased, which directly proved the regulation effect of TET2 on FAO (Fig. 5D). TET2 is a demethylase that mainly regulates the methylation of gene promoters [28]. So, we further screened the TET2-enriched DNA fragments by CUT & Tag assay. 26.46 % of the TET2 binding sites were promoters (Fig. 5E), and all the binding sites were mainly located in the transcript start site (Fig. 5F and G). As carnitine palmitoyl transferase 1A (CPT1A) was the rate-limiting enzyme of FAO, we investigated the enrichment of TET2 in CPT1A. The result showed that TET2 was significantly enriched in the promoter of CPT1A (Fig. 5H). Furthermore, the expression level of CPT1A was significantly decreased with the silence of TET2 in ECs (Fig. 5I). These results indicated that CPT1A was a direct target of TET2. We further locally overexpressed TET2 in adipose tissue (Fig. 5J). This resulted in increased browning of the adipose tissue and this effect was completely inhibited by the FAO inhibitor, etomoxir (Fig. 5K). At the same time, supplemented acetate (replaced the depleted acetyl-CoA derived from FAO by metabolizing into acetyl-CoA) effectively restored the vascular rarefaction caused by endothelial TET2 deficiency (Supplementary Fig. S9). These results suggested that TET2 regulated adipose tissue browning through CPT1A.

3.6. NRF2 recruits TET2 to regulate FAO

TET2 normally needs co-factors for binding to DNA, such as transcription factors [29]. NRF2, nuclear factor erythroid 2-related factor 2, has been confirmed as the essential for adaptative browning of white adipocytes [30]. Previous studies also indicated that the activator of NRF2 could alleviate HFD-induced obesity [31] and the interaction between TET2 and KEAP1, which was the inhibitor of NRF2 [32]. This prompted us to speculate whether TET2 could directly bind to NRF2 to exert its metabolic function. First, the protein binding sites of TET2 and NRF2 were predicted using Gramm-X (Fig. 6A). Then, the direct binding was further confirmed by immunoprecipitation (Fig. 6B and C). In order to elucidate the specificity of the TET2-NRF2 interaction, plasmids containing different domains of TET2 and NRF2 were constructed (Fig. 6D). The interaction between TET2 and NRF2 was detected in ectopically expressed HEK293T cells (Fig. 6E and F). To further determine the binding sites of TET2 and NRF2, two deletion mutant plasmids of TET2 were expressed with NRF2 in HEK293T cells. Co-IP analysis revealed that the CD domain of TET2 was essential for NRF2 binding. (Fig. 5G). Subsequently, we investigated their effects on DNA methylation. The results of ELISA assay showed that there was no difference in global DNA Methylation with the silence of TET2 (Fig. 5H). MSP experiments were further conducted to demonstrate that TET2 could regulate the methylation of BMP4 and CPT1A promoters (Fig. 6I). To determine the effect of NRF2 on regulating the expression of CPT1A and BMP4, JASPAR was used to predict the binding sites of NRF2 and the promoters of CPT1A and BMP4. The results showed that 3 sites of CPT1A promoter and 2 sites of BMP4 promoter could be bound by NRF2 (Fig. 6J). In order to explore whether TET2 and NRF2 jointly regulated BMP4 and CPT1A, we conducted further investigation. RT-qPCR analysis revealed that the effects of TET2-mediated activation of CPT1A and BMP4 were significantly diminished following NRF2 knockdown (Fig. 6K). Meanwhile, the effects of NRF2 activator, bardoxolone methyl, were significantly inhibited by TET2 siRNA (Fig. 6L). Overall, the above results demonstrated that TET2 regulated BMP4 and CPT1A through recruitment of NRF2.

4. Discussion

ECs have been extensively investigated as integral constituents of vascular structures, traditionally perceived as having a passive role in

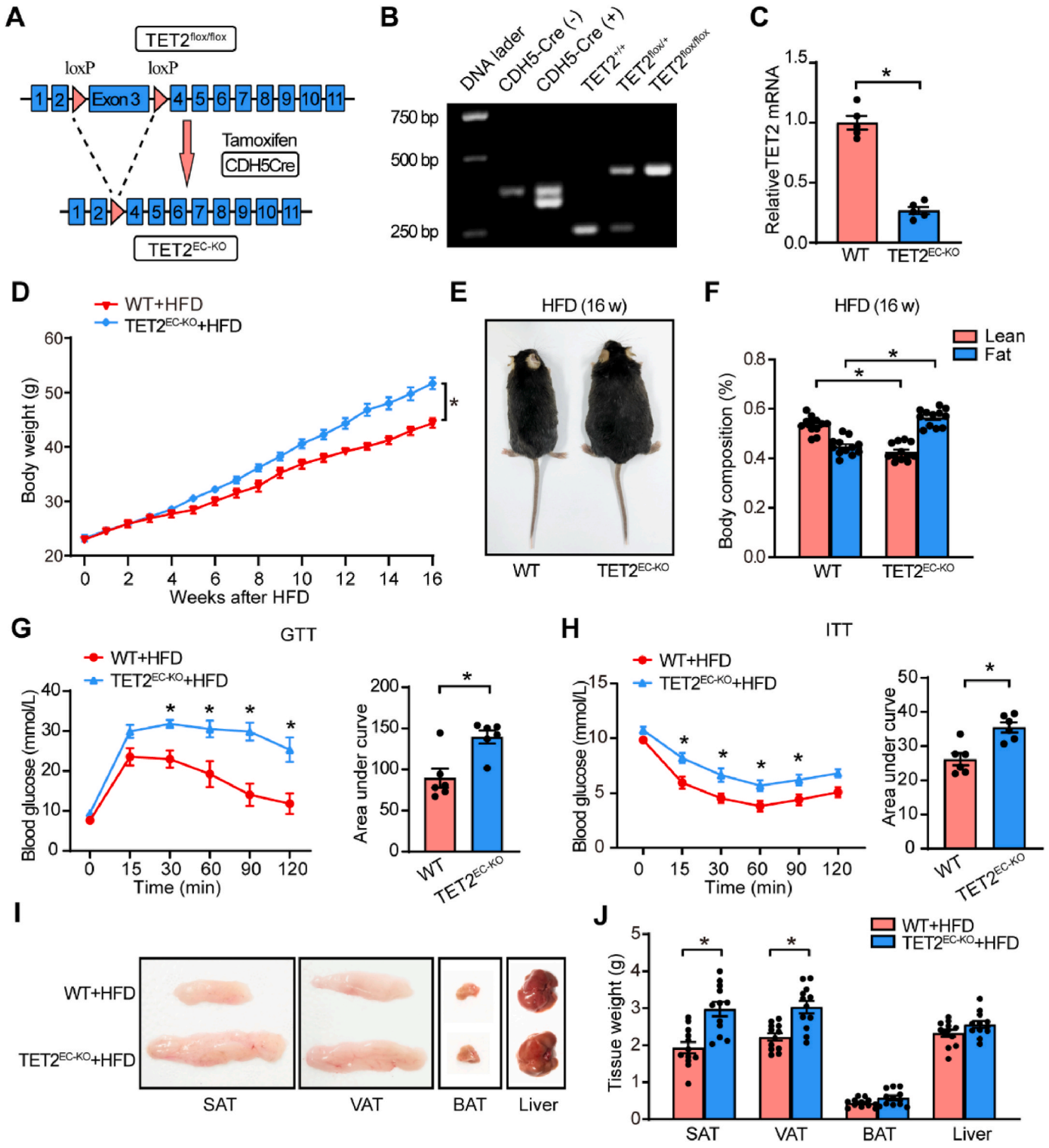

Fig. 2. Loss of endothelial TET2 aggravates HFD-induced obesity. A, Establishment diagram of $TET2^{EC-KO}$ mice. **B**, Identification of different genotypes of mice. **C**, qPCR of ECs isolated from SAT. n = 5 mice/group. **D**, Body weight curve of WT and $TET2^{EC-KO}$ mice fed with HFD. n = 12 mice/group. **E**, Representative images of whole-body pictures from WT and $TET2^{EC-KO}$ mice fed with HFD for 16 weeks. **F**, Body compositions of WT and $TET2^{EC-KO}$ mice with HFD were measured by Echo MRI. n = 12 mice/group. **G** and **H**, GTT (G) and ITT (H) of mice fed with HFD for 16 weeks. n = 6 mice/group. **I**, Representative images of SAT, VAT, BAT and liver from WT and $TET2^{EC-KO}$ mice fed with HFD for 16 weeks. **J**, Weight of SAT, VAT, BAT and liver from WT and $TET2^{EC-KO}$ mice fed with HFD for 16 weeks. All data are mean ± SEM. C, D, J, unpaired Student's *t*-test. F, G, H, Two-way ANOVA with Bonferroni post hoc test. $^*P < 0.05$.

maintaining systemic metabolic equilibrium [33]. Targeting the vasculature of adipose tissue has been proposed as a promising strategy for treating metabolic disorders, such as obesity [34]. In our study, we demonstrated that TET2 deficiency in ECs contributed to the development of obesity in mice feeding with HFD. The $TET2^{EC-KO}$ mice exhibited reduced insulin sensitivity, vascularization, and browning of adipose tissue. To clarify the underlying mechanisms, we identified that TET2 played a critical role in regulating obesity by influencing

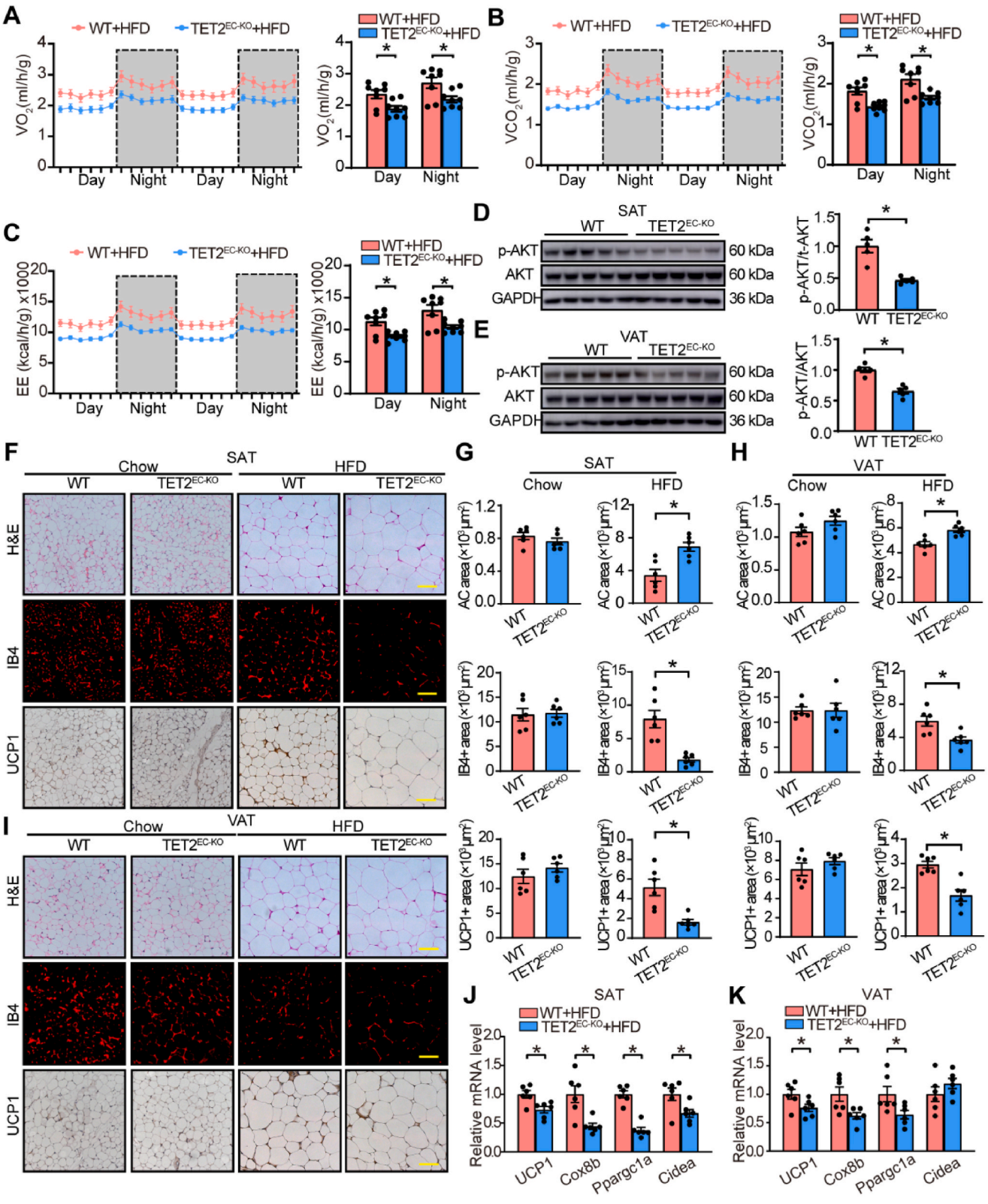

Fig. 3. Endothelial TET2 deficiency disrupts metabolism and WAT browning in HFD-induced obesity. A-C, Whole body oxygen consumption rate (A), carbon dioxide production date (B), and energy expenditure (C) normalized to body weight. n = 8 mice/group. **D** and **E**, Protein level of *p*-AKT and AKT in SAT (D) and VAT (E) from WT and TET2^{EC-KO} mice with HFD for 16 weeks. n = 5 mice/group. **F** and **I**, Representative images of adipose tissue (H&E), microvessels (IB4, red), and UCP1 staining in SAT (F) and VAT (G) from WT or TET2^{EC-KO} mice with chow diet or HFD for 16 weeks. Scale bar = 50 μm. **G** and **H**, Quantifications of adipocyte area, IB4 positive area and UCP1 positive area in SAT (G) and VAT (H) from WT or TET2^{EC-KO} mice fed with chow diet or HFD for 16 weeks. n = 6 mice/group. **J** and **K**, Relative mRNA levels of thermogenesis-related genes in SAT (J) and VAT (K) from WT and TET2^{EC-KO} mice fed with HFD for 16 weeks. All data are mean ± SEM. A, B, C, D, E, G, H, J, K, unpaired Student's *t*-test. *$P < 0.05$. (For interpretation of the references to color in this figure legend, the reader is referred to the Web version of this article.)

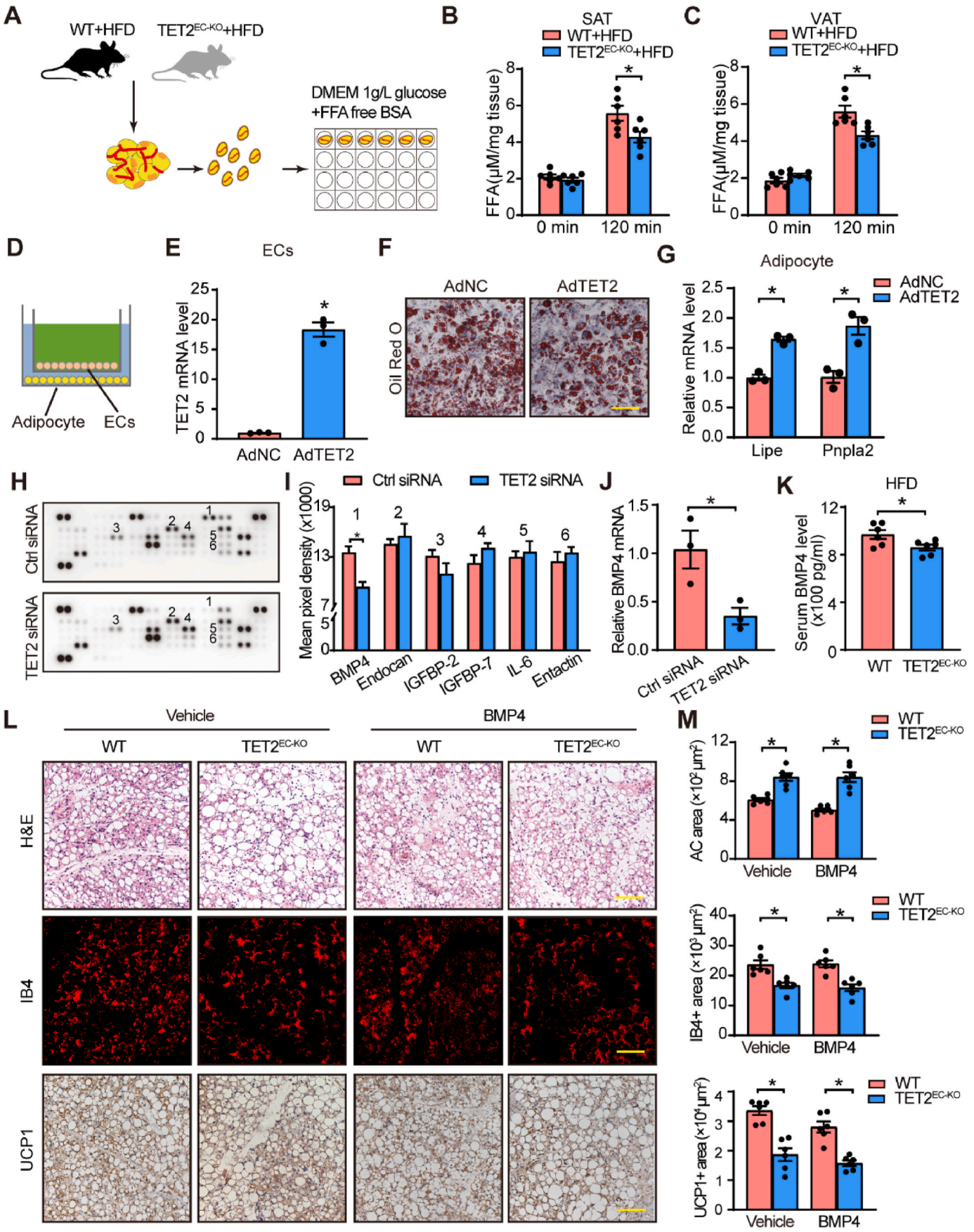

(caption on next page)

Fig. 4. Endothelial TET2 modulates lipolysis through secretion of BMP4. A, Diagram of in vivo WAT explants assay. **B** and **C**, FFA level of SAT (B) and VAT (C) obtained from WT or $TET2^{EC-KO}$ mice at the time of 0 min or 120 min (n = 6 mice/group). **D**, Diagram of co-culture of bEnd.3 and adipocytes. **E**, qPCR analysis of bEnd.3 after overexpressing TET2 by adenovirus. n = 3/group. **F,** Representative images of oil red O staining in adipocytes after co-culturing with TET2 overexpressed bEnd.3. Scale bars = 50 μm. **G**, qPCR analysis of lipolysis-related genes in adipocytes after co-culturing with TET2 overexpressed bEnd.3. n = 3/group. **H**, Cell culture supernatants of HUVECs transfected with ctrl siRNA or TET2 siRNA were detected by human adipokine array kit. **I**, Relative mean pixel density of H was calculated. n = 3/group. **J**, Relative mRNA levels of BMP4 in HUVECs transfected with Ctrl siRNA or TET2 siRNA. n = 3/group. **K**, Serum BMP4 level of WT and $TET2^{EC-KO}$ mice with HFD for 16 weeks. n = 6 mice/group. **L**, Representative images of adipocyte morphology (H&E), microvessels (IB4, red), UCP1 staining in SAT from WT or $TET2^{EC-KO}$ mice with or without local injection of BMP4 in CL316243-treated model. **M**, Quantification of L. n = 6 mice/group. All data are mean ± SEM. E, G, I, J, K, unpaired Student's *t*-test. B, C, M, Two-way ANOVA with Bonferroni post hoc test. $^*P < 0.05$. (For interpretation of the references to color in this figure legend, the reader is referred to the Web version of this article.)

endothelial FAO and the secretion of BMP4, a signaling molecule that directly impacted adipocytes through paracrine signaling. In mice with TET2 overexpression, suppression of FAO using etomoxir leaded to significant inhibition of vascularization and browning. Overall, our findings reveal a novel mechanism through which the TET2-FAO pathway regulates the function and metabolism of adipose tissue.

TET2, a member of the Ten-Eleven Translocation family, has garnered significant attention in the context of obesity due to its crucial role in epigenetic regulation and metabolic homeostasis [35–37]. TET2 functions as a DNA demethylase, catalyzing the conversion of 5-methylcytosine to 5-hydroxymethylcytosine and further oxidized derivatives [38,39]. Recent findings indicate that somatic TET2 mutations in hematopoietic cells, which occur with aging, contribute to the exacerbation of insulin resistance in mice experiencing physiological aging as well as diet-induced obesity [40]. Furthermore, TET2 of myeloid cells is implicated in the regulation of adipogenesis and adipose tissue function, thus influencing obesity development and metabolic complications [37,41]. Our research takes a fresh perspective and enriches the study of TET2 in obesity. As obesity progresses in its early stages, ECs exhibit increased proliferation to accommodate tissue expansion. However, as the disease further advances, the capacity of ECs to proliferate diminishes, and endothelial TET2 may play a critical role in this process. Previous studies have found that TET2 deficiency in adipocytes disrupts adipogenesis [41]. Here, we find that endothelial TET2 regulates HFD-induced obesity by modulating white adipose browning and lipolysis of adipocytes, which provides valuable insights into potential therapeutic targets and strategies for managing obesity and its associated metabolic disorders. Further research is warranted to elucidate the precise mechanisms underlying TET2-mediated effects and explore its therapeutic potential in combating obesity.

Within the realm of obesity, endothelial FAO has emerged as a pivotal metabolic process with significant implications [42]. Obesity is characterized by an imbalance between energy intake and expenditure, resulting in excess adipose tissue accumulation. This adiposity expansion exerts detrimental effects on endothelial function and contributes to the development of cardiovascular complications [43,44]. ECs line the inner surface of blood vessels, playing a pivotal role in regulating vascular homeostasis and metabolic processes [45]. Recent research has shed light on the role of FAO in modulating the metabolic state of ECs, indicating that FAO is essential for EC proliferation [46]. Our research demonstrates that endothelial TET2 could directly regulate FAO by sensing changes in the microenvironment of adipose tissue and modulating the expression levels of CPT1A, which is the gate-keeper enzyme for the entry of long-chain fatty acids into mitochondria [47,48]. Understanding the intricate interplay between endothelial FAO and obesity-induced metabolic perturbations holds great potential for developing strategies aimed at improving endothelial function and metabolism.

Our study also reveals that endothelial TET2 not only regulates FAO through CPT1A but also modulates the production of the FAO substrate FFAs by regulating the secretion of BMP4. BMP4 is a signaling molecule that has gained considerable attention in the field of obesity research due to its intricate involvement in adipose tissue biology and metabolic regulation [49–51]. Studies have revealed dysregulated expression and activity of BMP4 in obesity, highlighting its significant role in adipogenesis, adipocyte function, and energy homeostasis [52]. BMP4 is known to influence the differentiation of preadipocytes into mature adipocytes, as increased BMP4 signaling promotes adipogenesis and adipocyte maturation [53]. Furthermore, BMP4 has been shown to modulate adipocyte metabolism by regulating lipid storage, lipolysis, and glucose uptake [54]. Importantly, BMP4 signaling is not limited to adipose tissue but also extends to other organs involved in metabolic regulation, such as the liver [55,56]. Our study also identifies hepatic lipid deposition in $TET2^{EC-KO}$ mice, which may be associated with the decrease of BMP4 (Supplementary Fig. S5A). Previous studies have suggested that BMP4 in adipose tissue is primarily secreted by adipocytes [49]. However, we indicate that ECs are also an important source of BMP4 and the results presented here connect the functions of BMP4 and TET2 in ECs during obesity. In response to the demands of EC proliferation, ECs secrete BMP4 to promote the lipolysis of adipocytes, thereby providing the FFAs required for ECs.

In contrast to TET1 and TET3, TET2 does not possess the CXXC DNA binding domain, which necessitates recruitment by transcription factors for its binding to DNA [29,30]. We further discover that NRF2 recruits TET2 to regulate the methylation of CPT1A and BMP4 promoters. NRF2 is known for its critical role in cellular antioxidant defense and detoxification pathways [30,57]. Emerging evidence suggests that NRF2 also plays a significant role in the regulation of adipose tissue homeostasis and energy metabolism. Activation of NRF2 signaling has been shown to attenuate adipocyte inflammation, oxidative stress, and insulin resistance, thereby potentially protecting against obesity-related complications [58,59]. Helber et al. demonstrated that the NRF2 agonist, dimethyl fumarate, could prevent obesity and adipocyte hypertrophy [60]. This beneficial effect is likely attributed, at least in part, to the action of endothelial cells. Combining our findings with Helber et al., this effect may be partially attributed to the action of NRF2 in ECs.

5. Conclusions

We reveal that endothelial TET2 can regulate WAT browning and fat tissue metabolism by changing the demand of FAO in adipose tissue ECs and regulating the lipolysis of adipocytes by BMP4 secretion from ECs. This work contributes to understanding the roles of ECs in obese and aging individuals, as well as the potential implication of TET2 in the treatment of obesity.

Funding

This work was supported by the Chinese National Natural Science Foundation (grant numbers 82270867, 82070230, 82270473 and 82201207); and the Shanghai Hospital Development Center Foundation (grant number SHDC22023223).

CRediT authorship contribution statement

Yefei Shi: Conceptualization, Data curation, Formal analysis, Methodology, Writing – original draft, Writing – review & editing. **Xinru Huang:** Conceptualization, Data curation, Formal analysis, Methodology, Writing – original draft, Writing – review & editing. **Yanxi Zeng:** Methodology, Writing – original draft. **Ming Zhai:** Data curation.

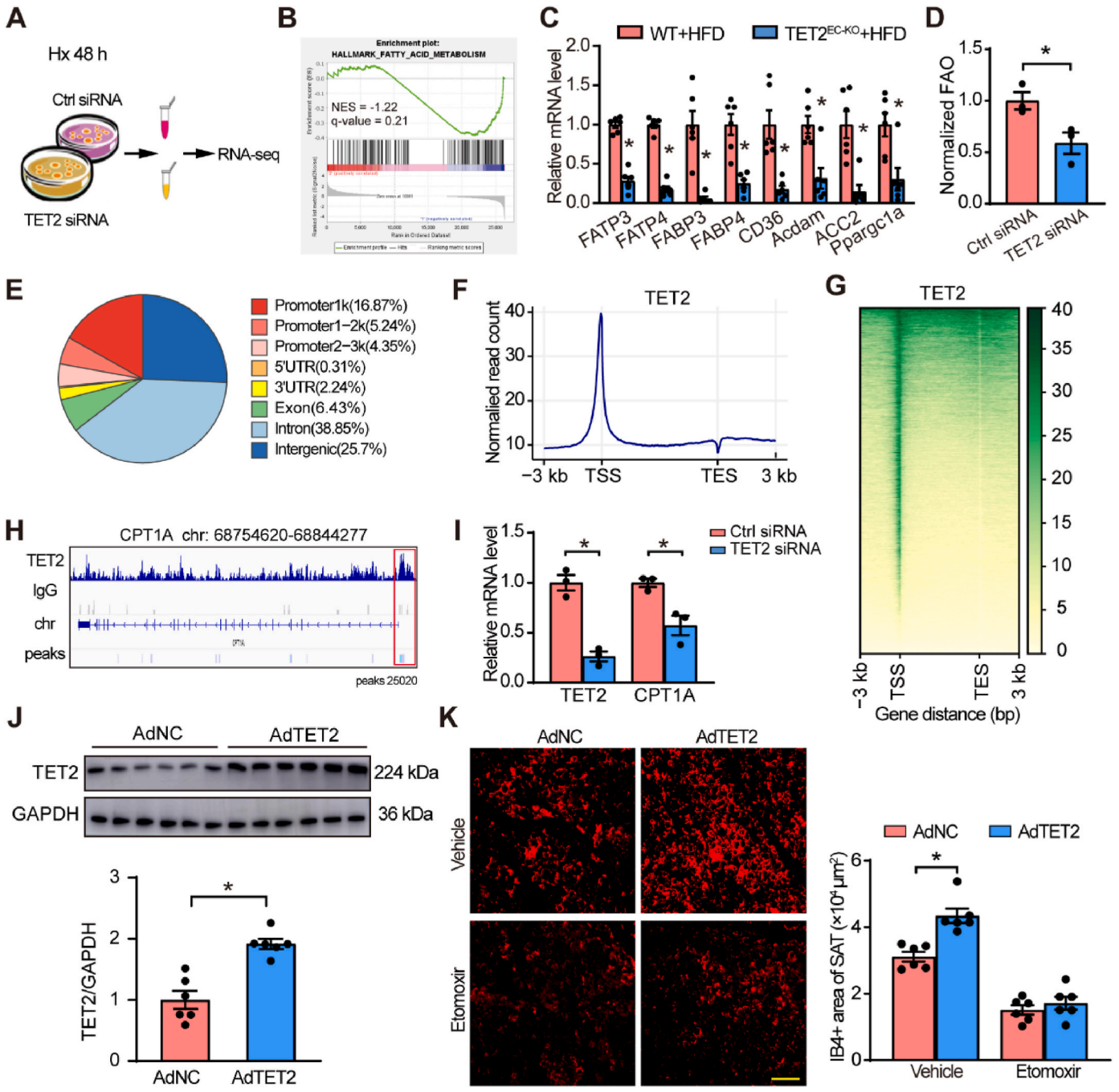

Fig. 5. TET2 regulates WAT browning via FAO in ECs. A, Diagram of RNA-seq of HUVECs transfected with TET2 siRNA under hypoxia for 48h. **B**, GSEA analysis of fatty acid metabolism in A. **C**, qPCR analysis of fatty acid metabolism-related genes in SAT from WT and $TET2^{EC-KO}$ mice. n = 6 mice/group. **D**, Fatty acid oxidation effect of TET2 siRNA in HUVECs was detected at 60-min time point. **E**, Genomic distribution of TET2 CUT & Tag peaks in HUVECs. **F**, Distribution of mapped TET2 peak locations are shown within 3 kb upstream of transcriptional start sites and 3 kb downstream of transcriptional end sites. **G**, CUT & Tag density heat map of TET2 enrichment in HUVECs. **H**, Illustration of TET2 binding on CPT1A promoter in HUVECs. **I**, qPCR analysis of HUVECs after transfected with ctrl siRNA or TET2 siRNA. n = 3/group. **J**, Western blot analysis of SAT from WT mice injected with AdNC or AdTET2 after 7 days. n = 6 mice/group. **K**, Representative images of microvessels (IB4, red) from SAT in CL316243-treateded model, which was overexpressed with or without TET2 adenovirus and treated either with vehicle or etomoxir. n = 6 mice/group. All data are mean ± SEM. C, D, I, J, unpaired Student's *t*-test. K, Two-way ANOVA with Bonferroni post hoc test. $^*P < 0.05$. (For interpretation of the references to color in this figure legend, the reader is referred to the Web version of this article.)

Hongyun Yao: Methodology. **Chang Liu:** Methodology. **Bo Li:** Methodology. **Shiyu Gong:** Methodology. **Qing Yu:** Methodology. **Jianhui Zhuang:** Methodology. **Yifan Zhao:** Methodology. **Liesheng Lu:** Methodology. **Bo Zhou:** Methodology. **Weixia Jian:** Conceptualization, Resources, Supervision, Writing – original draft, Writing – review & editing. **Wenhui Peng:** Conceptualization, Methodology, Resources, Supervision, Writing – original draft, Writing – review & editing.

Declaration of competing interest

The authors declare that they have no known competing financial interests or personal relationships that could have appeared to influence the work reported in this paper.

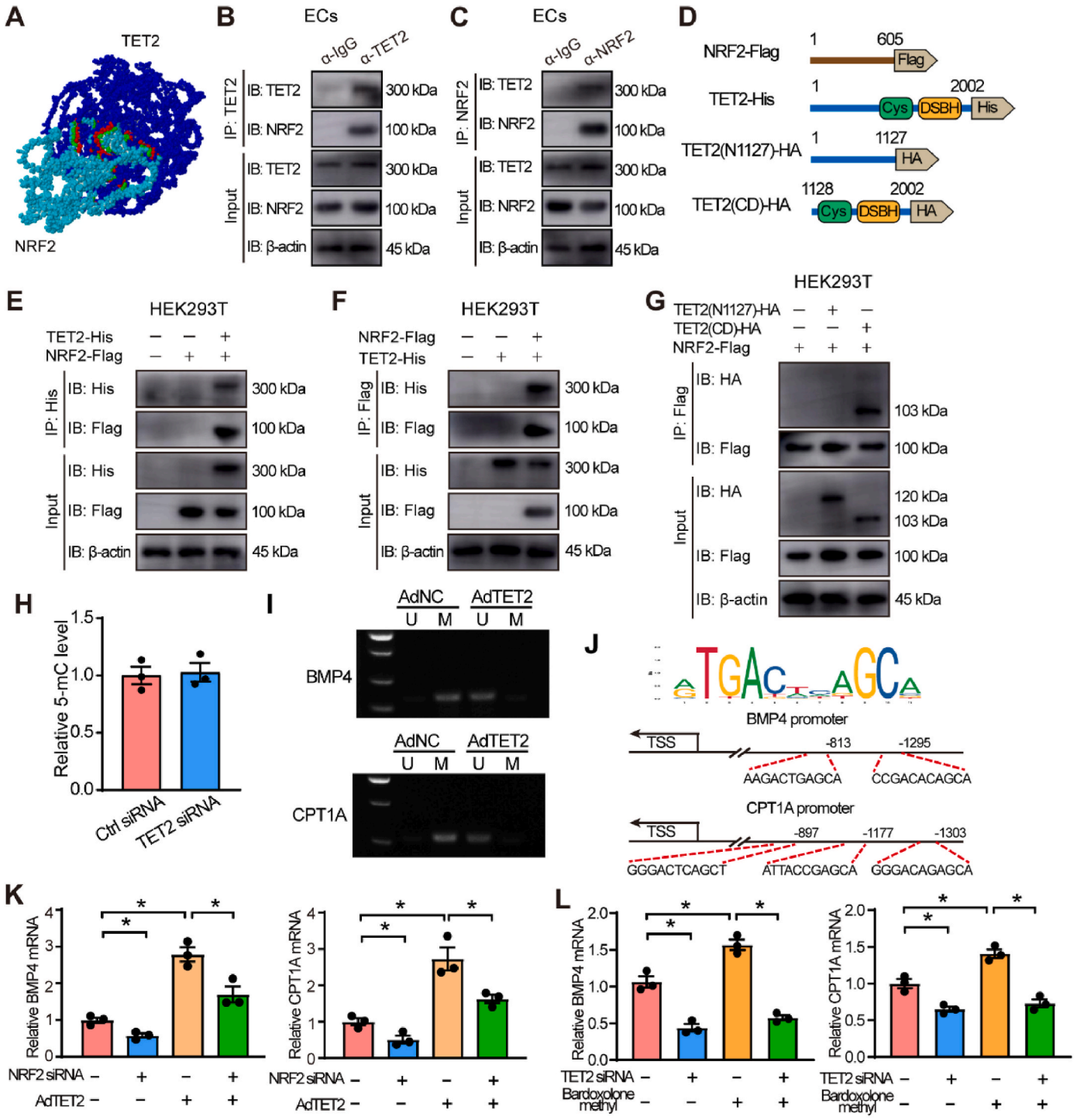

Fig. 6. NRF2 recruits TET2 to regulate FAO. A, Binding sites of TET2 and NRF2 were predicted using Gramm-X. Blue, TET2; Cyan, NRF2; Red, binding sites. **B** and **C**, Lysate of HUVECs was immunoprecipitated with anti-TET2 antibody (B) or anti-NRF2 antibody (C) and then immunoblotted with the indicated antibodies. **D**, Schematic illustration of different plasmids of TET2 and NRF2. **E** and **F**, TET2-His and NRF2-Flag were ectopically expressed in HEK293T and the lysate of HEK293T was immunoprecipitated with anti-His (E) antibody or anti-Flag antibody (F). **G**, NRF2 was ectopically expressed with different domains of TET2 HEK293T and the lysate of HEK293T was immunoprecipitated with anti-Flag antibody. **H**, The 5-mC levels of HUVECs transfected with or without TET2 siRNA. n = 3/group. **I**, The methylation status of BMP4 and CPT1A promoter in HUVECs treated with AdNC or AdTET2. **J**, Predict binding sites of NRF2 in the promoters of CPT1A and BMP4 by JASPAR. **K**. qPCR analysis of the mRNA expression levels of CPT1A and BMP4 in HUVECs infected with TET2 adenovirus in presence or absence of NRF2 siRNA. n = 3/group. **L**. qPCR analysis of the mRNA expression levels of CPT1A and BMP4 in HUVECs treated with bardoxolone methyl in presence or absence of TET2 siRNA. n = 3/group. All data are mean ± SEM. E, Two-way ANOVA with Bonferroni post hoc test. *$P < 0.05$. (For interpretation of the references to color in this figure legend, the reader is referred to the Web version of this article.)

Data availability

Data will be made available on request.

Acknowledgment

We thank Prof. Yanyun Gu (Department of Endocrinology, Ruijin Hospital, Shanghai Jiaotong University School of Medicine) for the technical support of body composition analysis and all the volunteers who participated in this study.

Appendix A. Supplementary data

Supplementary data to this article can be found online at https://doi.org/10.1016/j.redox.2023.103013.

References

[1] G.A. Colditz, W.C. Willett, A. Rotnitzky, J.E. Manson, Weight gain as a risk factor for clinical diabetes mellitus in women, Ann. Intern. Med. 122 (1995) 481–486, https://doi.org/10.7326/0003-4819-122-7-199504010-00001.

[2] P. Poirier, T.D. Giles, G.A. Bray, Y. Hong, J.S. Stern, F.X. Pi-Sunyer, et al., Obesity and cardiovascular disease: pathophysiology, evaluation, and effect of weight loss: an update of the 1997 American heart association scientific statement on obesity and heart disease from the obesity committee of the Council on nutrition, physical activity, and metabolism, Circulation 113 (2006) 898–918, https://doi.org/10.1161/CIRCULATIONAHA.106.171016.

[3] M. Blüher, Obesity: global epidemiology and pathogenesis, Nat. Rev. Endocrinol. 15 (2019) 288–298, https://doi.org/10.1038/s41574-019-0176-8.

[4] O. Gealekman, N. Guseva, C. Hartigan, S. Apotheker, M. Gorgoglione, K. Gurav, et al., Depot-specific differences and insufficient subcutaneous adipose tissue angiogenesis in human obesity, Circulation 123 (2011) 186–194, https://doi.org/10.1161/CIRCULATIONAHA.110.970145.

[5] I. Shimizu, T. Aprahamian, R. Kikuchi, A. Shimizu, K.N. Papanicolaou, S. MacLauchlan, et al., Vascular rarefaction mediates whitening of brown fat in obesity, J. Clin. Invest. 124 (2014) 2099–2112, https://doi.org/10.1172/JCI71643.

[6] J.G. McCarron, M.D. Lee, C. Wilson, The endothelium solves problems that endothelial cells do not know exist, Trends Pharmacol. Sci. 38 (2017) 322–338, https://doi.org/10.1016/j.tips.2017.01.008.

[7] A. Cartier, T. Leigh, C.H. Liu, T. Hla, Endothelial sphingosine 1-phosphate receptors promote vascular normalization and antitumor therapy, Proc. Natl. Acad. Sci. U. S. A. 117 (2020) 3157–3166, https://doi.org/10.1073/pnas.1906246117.

[8] K. Sun, I. Wernstedt Asterholm, C.M. Kusminski, A.C. Bueno, Z.V. Wang, J. W. Pollard, et al., Dichotomous effects of VEGF-A on adipose tissue dysfunction, Proc. Natl. Acad. Sci. U. S. A. 109 (2012) 5874–5879, https://doi.org/10.1073/pnas.1200447109.

[9] M. Grunewald, S. Kumar, H. Sharife, E. Volinsky, A. Gileles-Hillel, T. Licht, et al., Counteracting age-related VEGF signaling insufficiency promotes healthy aging and extends life span, Science (2021) 373, https://doi.org/10.1126/science.abc8479.

[10] K.D. Rasmussen, K. Helin, Role of TET enzymes in DNA methylation, development, and cancer, Genes Dev. 30 (2016) 733–750, https://doi.org/10.1101/gad.276568.115.

[11] S.C. Wu, Y. Zhang, Active DNA demethylation: many roads lead to Rome, Nat. Rev. Mol. Cell Biol. 11 (2010) 607–620, https://doi.org/10.1038/nrm2950.

[12] M. Buscarlet, S. Provost, Y.F. Zada, A. Barhdadi, V. Bourgoin, G. Lépine, et al., DNMT3A and TET2 dominate clonal hematopoiesis and demonstrate benign phenotypes and different genetic predispositions, Blood 130 (2017) 753–762, https://doi.org/10.1182/blood-2017-04-777029.

[13] G. Genovese, A.K. Kähler, R.E. Handsaker, J. Lindberg, S.A. Rose, S.F. Bakhoum, et al., Clonal hematopoiesis and blood-cancer risk inferred from blood DNA sequence, N. Engl. J. Med. 371 (2014) 2477–2487, https://doi.org/10.1056/NEJMoa1409405.

[14] J.J. Fuster, M.A. Zuriaga, V. Zorita, S. MacLauchlan, M.N. Polackal, V. Viana-Huete, et al., TET2-Loss-of-Function-Driven clonal hematopoiesis exacerbates experimental insulin resistance in aging and obesity, Cell Rep. 33 (2020), 108326, https://doi.org/10.1016/j.celrep.2020.108326.

[15] H.S. Kaya-Okur, D.H. Janssens, J.G. Henikoff, K. Ahmad, S. Henikoff, Efficient low-cost chromatin profiling with CUT&Tag, Nat. Protoc. 15 (2020) 3264–3283, https://doi.org/10.1038/s41596-020-0373-x.

[16] O. Bondareva, J.R. Rodríguez-Aguilera, F. Oliveira, L. Liao, A. Rose, A. Gupta, K. Singh, et al., Single-cell profiling of vascular endothelial cells reveals progressive organ-specific vulnerabilities during obesity, Nat. Metab. 4 (2022) 1591–1610, https://doi.org/10.1038/s42255-022-00674-x.

[17] Y. Shi, B. Li, X. Huang, W. Kou, M. Zhai, Y. Zeng, et al., Loss of TET2 impairs endothelial angiogenesis via downregulating STAT3 target genes, Cell Biosci. 13 (2023) 12, https://doi.org/10.1186/s13578-023-00960-5.

[18] S. Zhi, Z. Congcong, G. Zhiling, Q. Yihan, X. Yijing, L. Guanjie, et al., Quantitative proteomics of HFD-induced fatty liver uncovers novel transcription factors of lipid metabolism, Int. J. Biol. Sci. 18 (2022) 3298–3312, https://doi.org/10.7150/ijbs.71431.

[19] B. Mittendorfer, B.W. Patterson, G.I. Smith, M. Yoshino, S. Klein, β Cell function and plasma insulin clearance in people with obesity and different glycemic status, J. Clin. Invest. (2022) 132, https://doi.org/10.1172/JCI154068.

[20] J.J. Fuster, S. MacLauchlan, M.A. Zuriaga, M.N. Polackal, A.C. Ostriker, R. Chakraborty, et al., Clonal hematopoiesis associated with TET2 deficiency accelerates atherosclerosis development in mice, Science 355 (2017) 842–847, https://doi.org/10.1126/science.aag1381.

[21] S. Sano, K. Oshima, Y. Wang, S. MacLauchlan, Y. Katanasaka, M. Sano, et al., Tet2-Mediated clonal hematopoiesis accelerates heart failure through a mechanism involving the IL-1β/NLRP3 inflammasome, J. Am. Coll. Cardiol. 71 (2018) 875–886, https://doi.org/10.1016/j.jacc.2017.12.037.

[22] M. Agrawal, A. Niroula, P. Cunin, M. McConkey, V. Shkolnik, P.G. Kim, et al., TET2-mutant clonal hematopoiesis and risk of gout, Blood 140 (2022) 1094–1103, https://doi.org/10.1182/blood.2022015384.

[23] T. Seki, K. Hosaka, S. Lim, C. Fischer, J. Honek, Y. Yang, et al., Endothelial PDGF-CC regulates angiogenesis-dependent thermogenesis in beige fat, Nat. Commun. 7 (2016), 12152, https://doi.org/10.1038/ncomms12152.

[24] D. Bauters, M. Cobbaut, L. Geys, J. Van Lint, B. Hemmeryckx, H.R. Lijnen, Loss of ADAMTS5 enhances brown adipose tissue mass and promotes browning of white adipose tissue via CREB signaling, Mol. Metabol. 6 (2017) 715–724, https://doi.org/10.1016/j.molmet.2017.05.004.

[25] X. Tang, Y. Miao, Y. Luo, K. Sriram, Z. Qi, F.M. Lin, et al., Suppression of endothelial AGO1 promotes adipose tissue browning and improves metabolic dysfunction, Circulation 142 (2020) 365–379, https://doi.org/10.1161/CIRCULATIONAHA.119.041231.

[26] B. Gustafson, U. Smith, The WNT inhibitor Dickkopf 1 and bone morphogenetic protein 4 rescue adipogenesis in hypertrophic obesity in humans, Diabetes 61 (2012) 1217–1224, https://doi.org/10.2337/db11-1419.

[27] L.-A. Teuwen, N. Draoui, C. Dubois, P. Carmeliet, Endothelial cell metabolism: an update anno 2017, Curr. Opin. Hematol. 24 (2017) 240–247, https://doi.org/10.1097/MOH.0000000000000335.

[28] B. Cong, Q. Zhang, X. Cao, The function and regulation of TET2 in innate immunity and inflammation, Protein Cell 12 (2021) 165–173, https://doi.org/10.1007/s13238-020-00796-6.

[29] A. Seethy, K. Pethusamy, I. Chattopadhyay, R. Sah, A. Chopra, R. Dhar, et al., TETology: epigenetic mastermind in action, Appl. Biochem. Biotechnol. 193 (2021) 1701–1726, https://doi.org/10.1007/s12010-021-03537-5.

[30] M. Bauzá-Thorbrügge, E. Peris, S. Zamani, P. Micallef, A. Paul, S. Bartesaghi, et al., NRF2 is essential for adaptative browning of white adipocytes, Redox Biol. 68 (2023), 102951, https://doi.org/10.1016/j.redox.2023.102951.

[31] H.D.M. Valença, C.P. E Silva, L. de Brito Gitirana, S.S. Valença, M. Lanzetti, Beneficial effects of Ilex paraguariensis in the prevention of obesity-associated metabolic disorders in mice, Phytother Res. 36 (2) (2022) 1032–1042, https://doi.org/10.1002/ptr.7377.

[32] L.L. Chen, H.P. Lin, W.J. Zhou, C.X. He, Z.Y. Zhang, Z.L. Cheng, et al., SNIP1 recruits TET2 to regulate c-MYC target genes and cellular DNA damage response, Cell Rep. 25 (2018), https://doi.org/10.1016/j.celrep.2018.10.028.

[33] M. Graupera, M. Claret, Endothelial cells: new players in obesity and related metabolic disorders, Trends Endocrinol. Metabol. 29 (2018) 781–794, https://doi.org/10.1016/j.tem.2018.09.003.

[34] K. Sun, I. Wernstedt Asterholm, C.M. Kusminski, A.C. Bueno, Z.V. Wang, J. W. Pollard, et al., Dichotomous effects of VEGF-A on adipose tissue dysfunction, Proc. Natl. Acad. Sci. U. S. A. 109 (2012) 5874–5879, https://doi.org/10.1073/pnas.1200447109.

[35] T. Suzuki, T. Komatsu, H. Shibata, A. Tanioka, D. Vargas, R. Kawabata-Iwakawa, et al., Crucial role of iron in epigenetic rewriting during adipocyte differentiation mediated by JMJD1A and TET2 activity, Nucleic Acids Res. 51 (2023) 6120–6142, https://doi.org/10.1093/nar/gkad342.

[36] E.C. Fiedler, R.J. Shaw, AMPK regulates the epigenome through phosphorylation of TET2, Cell Metabol. 28 (2018) 534–536, https://doi.org/10.1016/j.cmet.2018.09.015.

[37] F. Bian, X. Ma, S.D. Villivalam, D. You, L.R. Choy, A. Paladugu, et al., TET2 facilitates PPARγ agonist-mediated gene regulation and insulin sensitization in adipocytes, Metabolism 89 (2018) 39–47, https://doi.org/10.1016/j.metabol.2018.08.006.

[38] Y.F. He, B.Z. Li, Z. Li, P. Liu, Y. Wang, Q. Tang, et al., Tet-mediated formation of 5-carboxylcytosine and its excision by TDG in mammalian DNA, Science 333 (2011) 1303–1307, https://doi.org/10.1126/science.1210944.

[39] S. Ito, L. Shen, Q. Dai, S.C. Wu, L.B. Collins, J.A. Swenberg, et al., Tet proteins can convert 5-methylcytosine to 5-formylcytosine and 5-carboxylcytosine, Science 333 (2011) 1300–1303, https://doi.org/10.1126/science.1210597.

[40] J.J. Fuster, K. Walsh, Somatic mutations and clonal hematopoiesis: unexpected potential new drivers of age-related cardiovascular disease, Circ. Res. 122 (2018) 523–532, https://doi.org/10.1161/CIRCRESAHA.117.312115.

[41] Y. Yoo, J.H. Park, C. Weigel, D.B. Liesenfeld, D. Weichenhan, C. Plass, et al., TET-mediated hydroxymethylcytosine at the Pparγ locus is required for initiation of adipogenic differentiation, Int. J. Obes. 41 (2017) 652–659, https://doi.org/10.1038/ijo.2017.8.

[42] E. Monelli, P. Villacampa, A. Zabala-Letona, A. Martinez-Romero, J. Llena, D. Beiroa, et al., Angiocrine polyamine production regulates adiposity, Nat. Metab. 4 (2022) 327–343, https://doi.org/10.1038/s42255-022-00544-6.

[43] M. Koenen, M.A. Hill, P. Cohen, J.R. Sowers, Obesity, adipose tissue and vascular dysfunction, Circ. Res. 128 (2021) 951–968, https://doi.org/10.1161/CIRCRESAHA.121.318093.

[44] J.J. Fuster, N. Ouchi, N. Gokce, K. Walsh, Obesity-induced changes in adipose tissue microenvironment and their impact on cardiovascular disease, Circ. Res. 118 (2016) 1786–1807, https://doi.org/10.1161/CIRCRESAHA.115.306885.
[45] X. Pi, L. Xie, C. Patterson, Emerging roles of vascular endothelium in metabolic homeostasis, Circ. Res. 123 (2018) 477–494, https://doi.org/10.1161/CIRCRESAHA.118.313237.
[46] S. Schoors, U. Bruning, R. Missiaen, K.C. Queiroz, G. Borgers, I. Elia, et al., Fatty acid carbon is essential for dNTP synthesis in endothelial cells, Nature 520 (2015) 192–197, https://doi.org/10.1038/nature14362.
[47] I.R. Schlaepfer, M. Joshi, CPT1A-mediated fat oxidation, mechanisms, and therapeutic potential, Endocrinology (2020) 161, https://doi.org/10.1210/endocr.
[48] N. Casals, V. Zammit, L. Herrero, R. Fadó, R. Rodríguez-Rodríguez, D. Serra, Carnitine palmitoyltransferase 1C: from cognition to cancer, Prog. Lipid Res. 61 (2016) 134–148, https://doi.org/10.1016/j.plipres.2015.11.004.
[49] B. Gustafson, A. Hammarstedt, S. Hedjazifar, J.M. Hoffmann, P.-A. Svensson, J. Grimsby, et al., BMP4 and BMP antagonists regulate human white and beige adipogenesis, Diabetes 64 (2015) 1670–1681, https://doi.org/10.2337/db14-1127.
[50] A. Hammarstedt, S. Gogg, S. Hedjazifar, A. Nerstedt, U. Smith, Impaired adipogenesis and dysfunctional adipose tissue in human hypertrophic obesity, Physiol. Rev. 98 (2018) 1911–1941, https://doi.org/10.1152/physrev.00034.2017.
[51] W. Mu, S. Qian, Y. Song, L. Yang, S. Song, Q. Yang, et al., BMP4-mediated browning of perivascular adipose tissue governs an anti-inflammatory program and prevents atherosclerosis, Redox Biol. 43 (2021), 101979, https://doi.org/10.1016/j.redox.2021.101979.
[52] S.W. Qian, Y. Tang, X. Li, Y. Liu, Y.Y. Zhang, H.Y. Huang, et al., BMP4-mediated brown fat-like changes in white adipose tissue alter glucose and energy homeostasis, Proc. Natl. Acad. Sci. U. S. A. 110 (2013) E798–E807, https://doi.org/10.1073/pnas.1215236110.
[53] H. Huang, T.J. Song, X. Li, L. Hu, Q. He, M. Liu, et al., BMP signaling pathway is required for commitment of C3H10T1/2 pluripotent stem cells to the adipocyte lineage, Proc. Natl. Acad. Sci. U. S. A. 106 (2009) 12670–12675, https://doi.org/10.1073/pnas.0906266106.
[54] R.K. Baboota, M. Blüher, U. Smith, Emerging role of bone morphogenetic protein 4 in metabolic disorders, Diabetes 70 (2021) 303–312, https://doi.org/10.2337/db20-0884.
[55] A. Kubo, Y.H. Kim, S. Irion, S. Kasuda, M. Takeuchi, K. Ohashi, et al., The homeobox gene Hex regulates hepatocyte differentiation from embryonic stem cell-derived endoderm, Hepatology 51 (2010) 633–641, https://doi.org/10.1002/hep.23293.
[56] X. Wang, B. Ma, X. Wen, H. You, C. Sheng, L. Bu, et al., Bone morphogenetic protein 4 alleviates nonalcoholic steatohepatitis by inhibiting hepatic ferroptosis, Cell Death Dis. 8 (2022) 234, https://doi.org/10.1038/s41420-022-01011-7.
[57] M. Yamamoto, T.W. Kensler, H. Motohashi, The KEAP1-NRF2 system: a thiol-based sensor-effector apparatus for maintaining redox homeostasis, Physiol. Rev. 98 (2018) 1169–1203, https://doi.org/10.1152/physrev.00023.2017.
[58] Z. Wang, Z. Zuo, L. Li, S. Ren, T. Gao, J. Fu, et al., Nrf2 in adipocytes, Arch Pharm. Res. (Seoul) 43 (2020) 350–360, https://doi.org/10.1007/s12272-020-01227-0.
[59] K.S. Schneider, J.Y. Chan, Emerging role of Nrf2 in adipocytes and adipose biology, Adv. Nutr. 4 (2013) 62–66, https://doi.org/10.3945/an.112.003103.
[60] HdM. Valença, C.P. E Silva, L. de Brito Gitirana, S.S. Valença, M. Lanzetti, Beneficial effects of Ilex paraguariensis in the prevention of obesity-associated metabolic disorders in mice, Phytother Res. 36 (2022) 1032–1042, https://doi.org/10.1002/ptr.7377.